Proc. Natl. Acad. Sci. USA
Vol. 96, pp. 1379–1384, February 1999
Biophysics

An approach to long-range electron transfer mechanisms in metalloproteins: *In situ* scanning tunneling microscopy with submolecular resolution

(azurin/spectroscopy)

ESBEN P. FRIIS*, JENS E. T. ANDERSEN*, YU. I. KHARKATS†, A. M. KUZNETSOV†, R. J. NICHOLS‡, J.-D. ZHANG*, AND JENS ULSTRUP*§

*Department of Chemistry, Technical University of Denmark, DK-2800 Lyngby, Denmark; †The A. N. Frumkin Institute of Electrochemistry of the Russian Academy of Sciences, Leninskij Prospect 31, 117071 Moscow, Russia; and ‡Department of Chemistry, University of Liverpool, Liverpool L69 3BX, England

Communicated by C. J. Ballhausen, University of Copenhagen, Charlottenlund, Denmark, December 1, 1998 (received for review July 7, 1998)

ABSTRACT ***In situ* scanning tunneling microscopy (STM) of redox molecules, in aqueous solution, shows interesting analogies and differences compared with interfacial electrochemical electron transfer (ET) and ET in homogeneous solution. This is because the redox level represents a deep indentation in the tunnel barrier, with possible temporary electronic population. Particular perspectives are that both the bias voltage and the overvoltage relative to a reference electrode can be controlled, reflected in spectroscopic features when the potential variation brings the redox level to cross the Fermi levels of the substrate and tip. The blue copper protein azurin adsorbs on gold(111) via a surface disulfide group. Well resolved *in situ* STM images show arrays of molecules on the triangular gold(111) terraces. This points to the feasibility of *in situ* STM of redox metalloproteins directly in their natural aqueous medium. Each structure also shows a central brighter contrast in the constant current mode, indicative of 2- to 4-fold current enhancement compared with the peripheral parts. This supports the notion of tunneling via the redox level of the copper atom and of *in situ* STM as a new approach to long-range electron tunneling in metalloproteins.**

Molecular long-range electron transfer (ET) in solid phases or liquid solution, in which the ET distance exceeds the structural extension of the donor and acceptor, has been in focus over the last decade and a half (1–5). Progress has rested on synthetic donor–acceptor molecules (1–3), metalloproteins (2, 4, 6, 7), and on new electrochemical systems in which electrons are brought to tunnel across well characterized, self-assembled films (8, 9). These achievements have prompted new theoretical efforts with notions such as directional tunneling along chemical bond networks (10), fluctuating tunnel barriers (11, 12), coherent and resonance ET (13), and self-consistent electronic–vibrational interaction (11).

In a parallel development, scanning tunneling and atomic force microscopy (STM and AFM, respectively) have opened exciting new perspectives for mapping molecular adsorbate patterns (14, 15). The primary basis for adsorption patterns in vacuum or air is imaging of small and intermediate-size adsorbate molecules with molecular and submolecular resolution (14–17), combined with theoretical frames for tunneling through adsorbate molecules based on different methodologies (17–21). There are also reported experimental approaches to functional mapping of intermediate-size molecules, most prominently in the form of correlations between the tunnel current and the bias voltage. Target adsorbates for *ex situ* STM imaging have been, for example, benzene (22, 23), methylazulenes (17, 24), C_{60} (25), alkyl and aryl thiolates (17, 21, 26–28), and transition metal phthalocyanins (29) on highly oriented pyrolytic graphite or crystalline surfaces of electronically "soft" metals compatible with the adsorbates. STM imaging at the solid/air interface to molecular and occasionally submolecular resolution also has been extended to biological macromolecules including DNA (30) and a number of redox and nonredox proteins (for an overview, see ref. 31). Functional properties addressed particularly have been the electrical potential distribution and conductivity patterns of the tunnel gap (21, 27–29), resonance tunneling via suitable highest occupied molecular orbitals, lowest unoccupied molecular orbitals, or (transition metal) redox levels (17–21), and the notion of orbital-specific mediation of the tunnel current (29).

Combination of STM with concepts of long-range ET in chemical and, particularly, metalloprotein systems must, however, give explicit attention to the fact that the natural medium for most chemical and biological reactivity is aqueous solution. Extension of STM/AFM to aqueous solution (*in situ* STM/AFM) is established (32, 33) but has raised issues related to adsorbate immobilization, ultrapure solutions, tip coating, independent tip and substrate potential control (32–34), and the fundamental STM and AFM phenomena. *In situ* STM offers, on the other hand, new electrochemical spectroscopic probes in addition to current–bias voltage relations, particularly the relation between the tunnel current and the overvoltage of both the tip and substrate electrodes relative to a common reference electrode. High-resolution mapping of adsorption patterns at the solid/aqueous solution interface by *in situ* STM has covered, for example, carbon monoxide (35), alkane thiols (36, 37), DNA bases (38–42), and other intermediate-size molecules such as porphyrins (43, 44) and tetramethylthiourea (45). *In situ* STM/AFM also has been brought to a level at which solid/aqueous solution structure and reactivity are coming within reach. Important observations are: (*i*) two-dimensional phase transitions of DNA base monolayers followed by cyclic voltammetry and high-resolution *in situ* STM (41, 42); (*ii*) imaging of molecular-reactive events, with oxidation of xanthin being a case (46); and (*iii*) *in situ* STM spectroscopy of metalloporphyrins based on relations between the tunnel current and either the bias voltage or the overvoltage (47, 48). Fundamental perspectives are the adsorbate energetics and electronic–vibrational coupling. These relate, importantly, to the individual molecules, as opposed to the statistical assemblies of chemical and electrochemical ET. This issue has been discussed elsewhere (49). Technological per-

The publication costs of this article were defrayed in part by page charge payment. This article must therefore be hereby marked "*advertisement*" in accordance with 18 U.S.C. §1734 solely to indicate this fact.

PNAS is available online at www.pnas.org.

Abbreviations: STM, scanning tunneling microscopy; ET, electron transfer; AFM, atomic force microscopy.

§To whom reprint requests should be addressed. e-mail: ju@kemi.dtu.dk.

spectives are related, for example, to surface catalytic processes, corrosion, or biosensors in action.

Biological macromolecules (proteins, enzymes) at the solid/aqueous solution interface have been addressed by AFM (50–53). Image resolution has been brought to a level at which conformational changes on enzyme–substrate complex formation, protein folding and unfolding (51), and force spectroscopic features have been recorded (50–52). *In situ* STM imaging of redox metalloproteins to molecular resolution also has been reported recently (31, 53–55). *In situ* STM of redox metalloproteins, with low-lying intermediate transition metal redox levels, holds new perspectives for long-range ET in metalloproteins and for conductivity changes induced by substrate binding such as that observed, for example, for the four-copper redox enzyme, ascorbate oxidase, in aqueous solution (57). The perspectives would extend to the elusive distinction between superexchange, coherent, and sequential ET mechanisms often discussed in ET science (1–7). Such data are not available presently but are in demand in view of the subtleties associated with the potential control and distribution in the gap region and with problems associated with robust layer configurations for electron exchange between metallic electrodes and adsorbed proteins (58).

In the present report we provide new high-resolution (submolecular) *in situ* STM images of the blue single-copper redox metalloprotein *Pseudomonas aeruginosa* azurin adsorbed on gold(111) surfaces, indicative of a particular role of the copper redox level. Azurins are well characterized blue single-copper ET proteins believed to have a role in bacterial respiration (59) or stress (60). A surface disulfide group (Cys-3–Cys-26 in *P. aeruginosa* azurin) opposite of the copper atom (Fig. 1) is suitable for linking azurin to gold by chemisorption and is connected to the copper atom by facile tunnel routes through the protein. Based on the crystallographic structure (Fig. 1) this would direct azurin to an adsorption configuration in which the disulfide–copper direction is close to perpendicular to the planar metal surface. Azurin shows diffusion-controlled cyclic voltammetry at pyrolytic graphite around the isoelectric point (pH 4.65) (53). Diffusion-controlled voltammetry is also found at polycrystalline gold but decays within 10–20 min. Monolayer formation appears on longer-time exposures as reflected by x-ray photoelectron spectroscopy, voltammetry associated with sulfur adsorption (reductive desorption), and *in situ* STM (ref. 53; J.-D.Z., E.P.F., and J.U., unpublished work). The azurins, therefore, are suitable target molecules for new approaches to long-range ET and two-dimensional protein adsorption based on *in situ* STM. We address first some theoretical expectations regarding correlations between the tunnel current and the bias voltage or overvoltage (49). We then report *in situ* STM images of *P. aeruginosa* azurin on gold(111) under specified conditions. The images show both a highly organized array of molecular-size structures and a characteristic submolecular feature, indicative of higher tunnel current in the central part of the molecule in which the copper atom is located. These *in situ* STM images of a robust metalloprotein array with submolecular resolution under specified conditions hold correspondence to contemporary views of long-range ET in metalloprotein systems and to theoretical approaches to resonance, coherent, and sequential tunnel mechanisms.

FIG. 1. Three-dimensional crystal structure of *P. aeruginosa* azurin. Coordinates are from ref. 61 and the Protein Data Bank. MOLSCRIPT graphic representation is shown (62). The copper atom is indicated by the sphere at the top, and the disulfide group is indicated by the two smaller, lighter spheres at the bottom.

MATERIALS AND METHODS

P. aeruginosa azurin was a gift from N. Bonander, Chalmers Technical University, Göteborg, Sweden, and was purified as in refs. 52 and 55. Millipore water and highest-purity reagents were used. Gold(111) substrates were prepared by annealing 400-nm gold layers on 1- × 1-cm glass plates (Berliner Glass, Berlin) in a gas flame for 5 min. The plates were allowed to cool for 1 or 2 min and then were covered by a drop of buffer solution, mounted in the STM cell, or transferred to a vial for azurin adsorption. Adsorption was accomplished by soaking the substrate in 1–10 mM azurin solution (50 mM ammonium

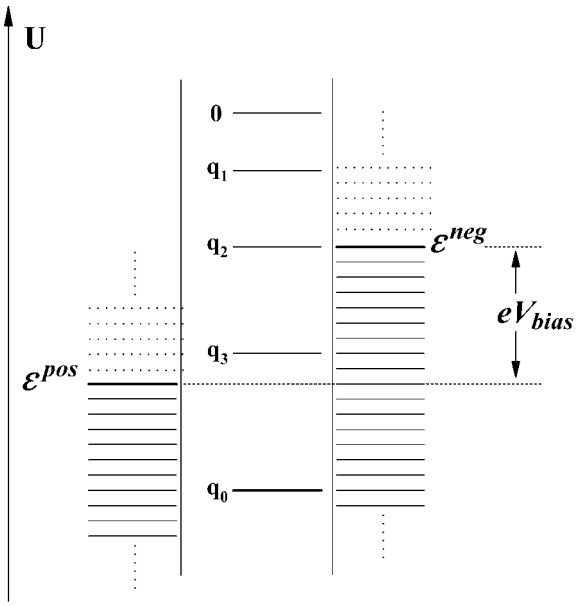

FIG. 2. Energy diagram of *in situ* three-level electronic–vibrational STM. Electronic energy manifolds of the positively, ε^{pos}, and negatively, ε^{neg}, biased electrode are coupled via the (initially vacant) molecular redox level. Fluctuations in the nuclear coordinate(s) q from the value $q = 0$ lower the level to values near the Fermi level, ε_F^{neg}, where ET occurs. Relaxation takes the filled molecular level to still lower values, where ET to the positively biased electrode occurs before full vibrational relaxation at $q = q_0$. q_1, q_2, and q_3 are intermediate nuclear configurations.

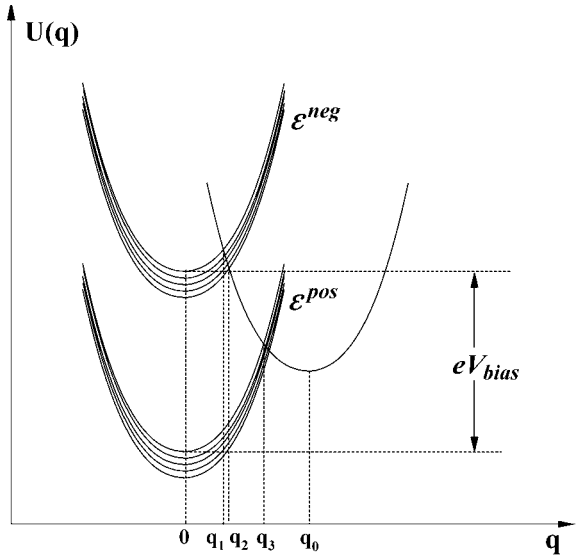

FIG. 3. Nuclear potential Gibbs free-energy surfaces corresponding to the electronic levels in Fig. 2.

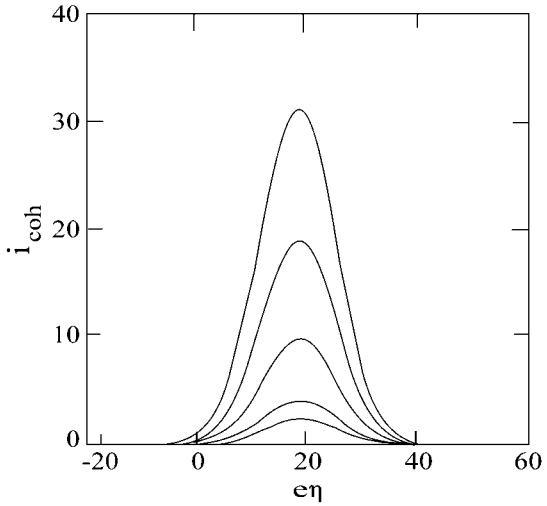

FIG. 5. Variation of the *in situ* STM current in Eq. **3**, with the overvoltage, at different bias voltages. Parameters are as in Fig. 4. Increasing currents correspond to the bias voltages 25, 50, 100, 150, and 200 mV. The maximum is at $e\eta \approx E_s$ for small bias voltage.

acetate, pH 4.65) for 1–24 hr. Blanks were prepared similarly, using azurin-free buffer.

A Rasterscope 3000 (Danish MicroEngineering, Copenhagen) STM instrument with independent control of substrate and tip potential was used. The fluid cell was cleaned in 75:25 wt/wt H_2SO_4/H_2O_2 overnight. The azurin-exposed gold samples were carefully flushed in buffer before assembling the cell, which contained pure buffer. Au/AuO_x reference electrodes were prepared by applying +4 V to a gold wire in 50 mM H_2SO_4 for 10 min and checked against an SCE before and after imaging. The counter electrode was a platinum wire. Tips were prepared by etching tungsten wire in a gold ring electrode with 2 M NaOH, followed by cleaning in water and covering by Apiezon wax. This suppresses Faradaic currents and ensures that only the outermost part of the tip is exposed. The commercial tip holder was modified to ensure sturdy mounting. After tip engagement the instrument was left scanning for 1 or 2 hr to minimize thermal drift.

RESULTS AND DISCUSSION

We consider first some energetic and dynamic features of long-range ET through a redox level in *in situ* STM. Fig. 2 shows schematically electron tunneling through a temporarily populated, low-lying electronic level representing the adsorbed redox molecule. This level, initially vacant, constitutes a tunnel barrier indentation. Similar considerations apply to hole transfer, where the level is initially occupied and below the Fermi levels of the substrate and tip electronic continuum levels. The redox level in the *in situ* STM mode is, moreover, strongly coupled to nuclear motion in the protein and solvent. Fluctuations in the nuclear configurations take the redox level close to the Fermi level of the negatively biased electrode, ε_F^{neg}, where ET from the electrode levels, ε^{neg}, to the redox level can occur. This is also illustrated by the potential Gibbs free-energy configuration in Fig. 3 (49). The following ET step can occur in two patterns. If the tunnel factors are small (long ET distances), full vibrational relaxation of the occupied (re-

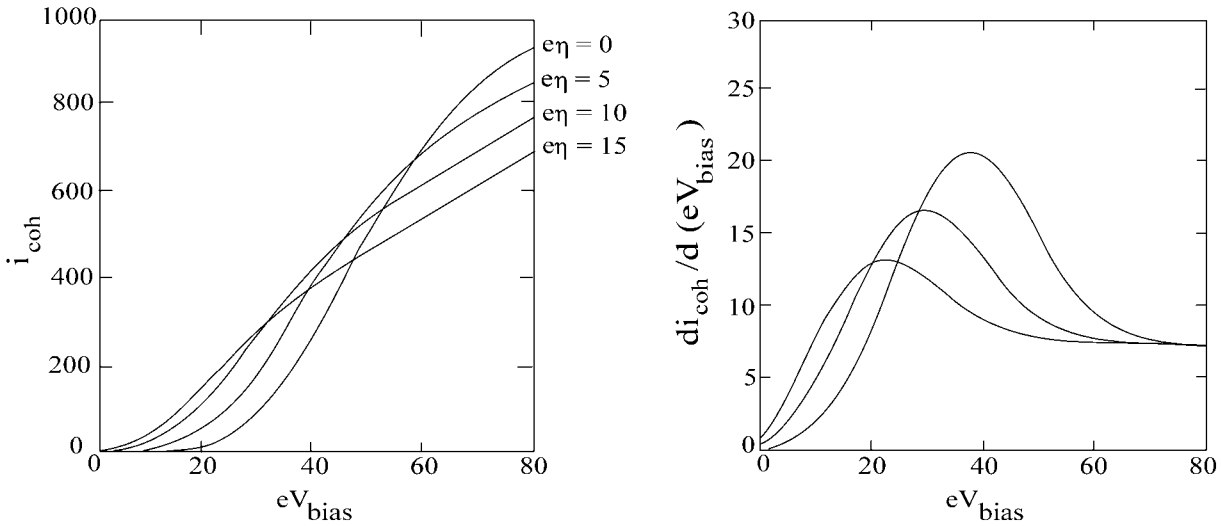

FIG. 4. (*Left*) Current–bias voltage relations for the configuration in Figs. 2 and 3. The correlations show the variation of the double integral in Eq. **3**, with the level densities and the approximately constant tunnel factors disregarded. Energy quantities in units of k_BT (=25 mV). $E_s = 20$ (0.5 V); $\alpha = 0.5$. The bias voltage range spanned thus is 2 V. The four curves correspond to the overvoltages indicated, with 0–15 corresponding to 0–0.375 V. The inflection points follow $e\eta$. (*Right*) Derivatives of the current–bias relation showing the structural feature as the redox level crosses ε_F^{neg}.

duced) level occurs and the second ET step to levels in the positively biased electrode, ε^{pos}, only follows after renewed thermal activation. The overall process is then equivalent to two consecutive electrochemical single ET. This could be called sequential two-step ET. Stronger electronic interaction between the redox center and the electrodes imposes another pattern. After the first ET, vibrational–conformational relaxation is initiated but the second ET now follows before relaxation is completed. This could be called coherent two-step ET because the two steps are now correlated, and tunnel features of both steps appear in the rate constant or tunnel current. Coherent ET is also encountered in ultrafast ET processes (63, 64). Superexchange would be a third mode in which ET is mediated through a high-energy intermediate state. As in long-range ET patterns of metalloproteins in homogeneous solution (1–7), the intermediate state in this mode is not populated but couples purely electronically the donor and acceptor states. This is favored relative to direct tunneling because of the much shorter nearest-neighbor distances in the superexchange mode.

Sequential and coherent ET are physically different. Current–voltage relations of the former can be framed by electrochemical single-ET theory, rooted in forms such as (5, 65)

$$i_{seq} \propto \int_{-\infty}^{\infty} d\varepsilon^{neg}\rho(\varepsilon^{neg})f(\varepsilon^{neg})[T_{neg}(\varepsilon^{neg};\ \eta;\ V_{bias})]^2 \times \exp\left\{-\frac{[E_s - e\eta - \alpha eV_{bias} - (\varepsilon^{neg} - \varepsilon_F^{neg})]^2}{4E_s k_B T}\right\}, \quad [1]$$

where $\rho(\varepsilon^{neg})$ is the level density, $f(\varepsilon^{neg})$ is the Fermi function, E_s is the nuclear reorganization Gibbs free energy, η is the overvoltage, V_{bias} is the bias voltage, and α is the fraction of the bias voltage at the redox center. e is the electronic charge, k_B is Boltzmann's constant, and T is temperature. $T_{neg}(\varepsilon^{neg};\ \eta;\ V_{bias})$ is the electron exchange factor between the electrode and the molecule. A simple form is

$$T_{neg}(\varepsilon^{neg};\ \eta;\ V_{bias}) \approx T^{o}_{neg} \exp\left\{-\frac{1}{\hbar} \times \sqrt{2m_e[U_{neg} + e\eta - \alpha eV_{bias} - (\varepsilon^{neg} - \varepsilon_F^{neg})]}a_{neg}\right\}, \quad [2]$$

where m_e is the electronic mass, a_{neg} is the tunnel gap, U_{neg} is the barrier height at equilibrium counted from ε_F^{neg}, and T^{o}_{neg} is an energy quantity independent of ε^{neg}, η, and V_{bias}. Eq. **1** extends to *in situ* STM in the sequential two-ET mode when the rate-determining step is ET from the negatively biased electrode to the molecule. When the second ET step is rate determining, the first step is equilibrated. The overall current is still given by a form similar to Eq. **2** but that now includes the equilibrium constant for the first step.

The coherent two-step tunnel current is (49)

$$i_{coh} \propto \int_{-\infty}^{\infty} d\varepsilon^{neg} \int_{-\infty}^{\varepsilon^{neg}} d\varepsilon^{pos}\ \rho(^{neg})\rho(\varepsilon^{pos})f(\varepsilon^{neg})[1 - f(\varepsilon^{pos})] \times [T_{neg}(\varepsilon^{neg};\ \eta;\ V_{bias})]^2[T_{pos}(\varepsilon^{pos};\ \eta;\ V_{bias})]^2 \times \exp\left\{-\frac{[E_s - e\eta - \alpha eV_{bias} - (\varepsilon^{neg} - g_F^{neg})]^2}{4E_s k_B T}\right\}, \quad [3]$$

where the superscript *pos* refers to the positively biased electrode. $T_{pos}(\varepsilon^{pos};\eta;V_{bias})$ can be given a form equivalent to Eq. **2**. Eqs. **1** and **3** show some important differences. Only the tunnel factor of the rate-determining step appears in the sequential mode. On the other hand, coherence is reflected in Eq. **3** by tunnel factors of both transitions. Eq. **3** thus represents electronic propagation from the negatively to the positively biased electrode via the molecular redox level. In contrast to the purely electronic role of intermediate levels in most approaches to long-range ET in metalloprotein (1–7), the intermediate redox level in the coherent mode is strongly coupled to the nuclear environment. The propagation therefore takes a more composite form involving the sequence: initial state nuclear activation → first electronic transition → partial intermediate-state vibrational relaxation → second electronic transition → final-state vibrational relaxation. The electronic factors in Eq. **3** finally can be brought to incorporate explicitly additional features of purely electronic propagation through individual amino acid residues or other intermediate group states. As noted, in contrast to much more common *ex situ* STM, *in situ* STM holds, moreover, the option of varying both the bias voltage and the overvoltage of both electrodes relative to a common reference electrode, at fixed bias voltage. The overvoltage dependence in the sequential two-ET mode then follows electrochemical single-ET behavior reaching, particularly, a plateau as $|e\eta| \rightarrow E_s$. In contrast, both voltage variations in coherent two-step tunneling show features of single-molecule spectroscopy (49). Fig. 4 shows current–bias voltage relations calculated on the basis of Eq. **3** in which an inflection point appears as the redox level traverses ε_F^{neg}. A maximum appears in the same potential region in the current–overvoltage relation (Fig. 5). The latter is approximately Gaussian at small bias voltage. Both relations have been observed. Tao observed a maximum in the effective height–overvoltage correlation for iron protoporphyrin IX adsorbed at highly oriented pyrolytic graphite (47), and Lindsay and associates found maxima in the derivative current–bias voltage relations for several metalloporphyrins tethered to gold(111) (48). The following discussion relates particularly to *P. aeruginosa* azurin on gold(111), where the crucial role of the metal

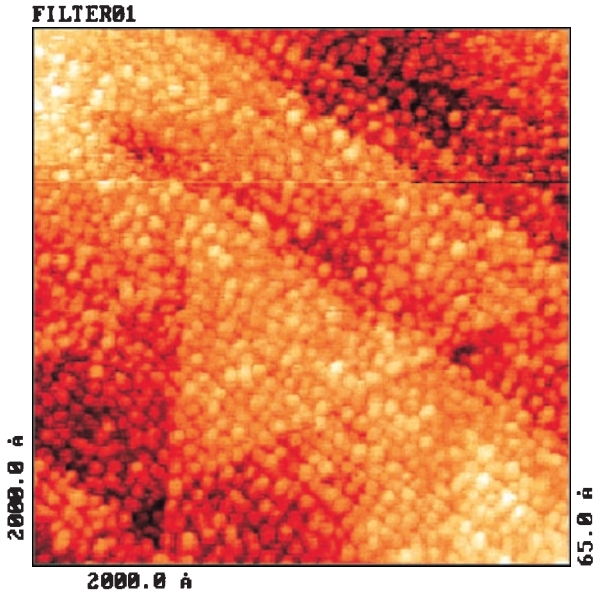

FIG. 6. *In situ* STM image of preadsorbed *P. aeruginosa* azurin on gold(111) (50 mM ammonium acetate, pH 4.65). Tunnel current = 2 nA. Substrate potential = −400 mV (Au/AuO_x) or +450 mV (SCE). Bias voltage = 400 mV. Each of the small structures corresponds in size to the crystallographic molecular adsorbate dimension, and the image is indicative of the formation of a highly ordered array of adsorbed azurin molecules. Each molecular-size structure also exhibits a central submolecular feature of brighter contrast, indicative of higher tunneling conductivity through this part of the molecule (cf. Fig. 7). A triangular gold(111) terrace is visible under the adsorbate layer.

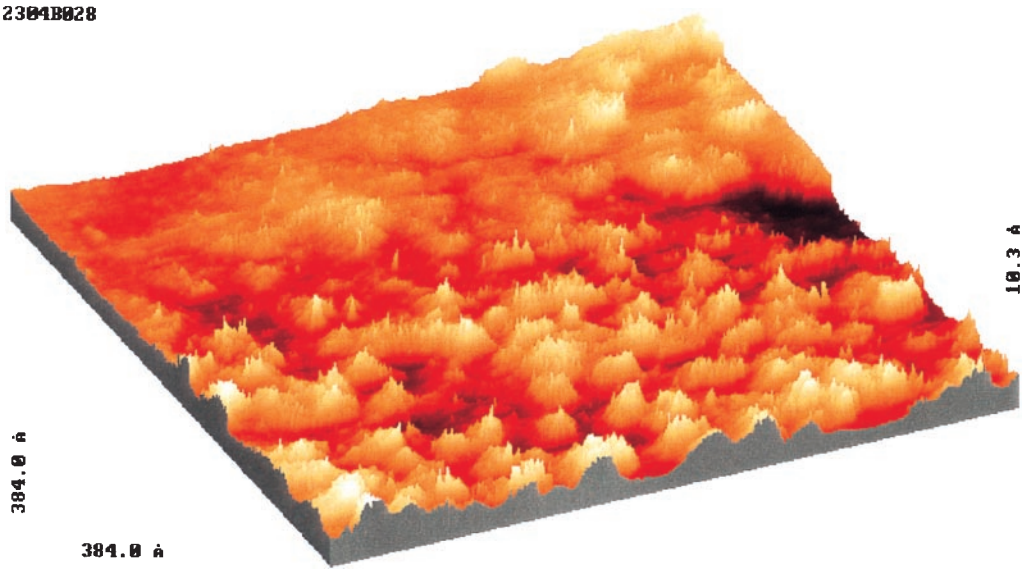

FIG. 7. High-resolution *in situ* STM image of adsorbed azurin on gold(111). Individual molecules and a submolecular central feature of brighter contrast are clearly visible. Conditions are as in Fig. 6.

center is reflected in an interesting submolecular image feature.

Figs. 6 and 7 show representative *in situ* STM images. Fig. 6 shows that well resolved, highly ordered, two-dimensional arrays can form. The arrays follow, interestingly, the triangular gold(111) substrate terraces, which can be distinguished underneath the protein adsorbate. The lateral size of each adsorbate structure is close to the crystallographic size of azurin (3–4 nm). This compatibility points to good adsorbate ordering and differs in this respect from *in situ* STM of covalently immobilized horse heart cytochrome *c*, where mostly larger lateral sizes are encountered (54). The vertical dimension of adsorbed *P. aeruginosa* azurin tends to be smaller than the crystallographic size. Height calibration is, however, sensitive to the "matter" in the tunnel gap and straightforwardly cannot be transferred between different environments. The apparent discrepancy can also reflect that the lowest heights between the molecular-size structures may not represent the bare electrode but, rather, regions of contact between neighboring molecules.

Fig. 7 shows another feature related to the discussion above. Each molecular-size structure has the shape of a cone standing on its base, rather than the smooth, ellipsoidal crystallographic shape of azurin (Fig. 1). A central region of brighter contrast is seen in each structure, with an apparent height 2- to 4-fold larger than in the peripheral parts. The images in Figs. 6 and 7 were recorded in the constant current mode. Brighter contrasts therefore represent regions of high-tunneling probability in which the tip is retracted from the surface. The submolecular feature in Figs. 6 and 7 is then indicative of enhanced tunneling through the central parts of each azurin molecule. Based on the theoretical notions above and supporting x-ray photoelectron spectroscopy and voltammetry (ref. 53; J.-D.Z., E.P.F., and J.U., unpublished work), an attractive frame, therefore, is that azurin is immobilized by chemisorption on gold(111) via the disulfide group and ET routes perpendicular to the surface (cf. Fig. 1) facilitate tunneling to the copper center. This feature is, however, not diagnostic with respect to the tunneling mechanism. The mechanism thus could involve tunneling assistance by temporary electron or hole population of the Cu(II/(I) redox level in sequential or coherent two-step ET, or this level could represent a barrier indentation or, in the notion of superexchange, facilitated but purely electronic assistance by the low-lying intermediate electronic level. In any case, tunneling would be enhanced in the protein region near the copper atom. These fully potentiostatically controlled *in situ* STM images are robust and show that imaging of metalloproteins directly in their natural aqueous medium to submolecular resolution is feasible.

Current–voltage relations for *in situ* STM of immobilized azurin on gold(111) presently are inconclusive (J.-D.Z., E.P.F., and J.U., unpublished work). Key observations are inhomogeneous broadening and robust image character-to-potential variation. The former accords with observations for covalently immobilized metalloporphyrins (48) and could be caused by stochastic effects as individual molecular functionality is followed. Weak sensitivity of the tunnel current-to-potential variation could be caused by competing tunneling mechanisms. Particularly, tunneling through an indented barrier (superexchange) would display a weaker potential dependence than sequential or coherent ET. In addition, the reorganization Gibbs free energy is small in STM configurations such as the one in Fig. 2 or 3. Representative values based on dielectric models are 0.25–0.30 eV (49) compared with ≈0.5 eV for a semiinfinite planar interface. Both competing tunneling mechanisms and low E_s would increase the effective metallic electronic level range and broaden the current–voltage relations.

Financial support from the Danish Natural and Technical Science Foundations, the Danish Research Academy, The Novo Nordisk, Carlsberg, and P. A. Fisker Foundations, the European Union program International Association for the Promotion of Cooperation with Scientists from the New Independent States of the Former Soviet Union, and the Russian Foundation for Basic Research is acknowledged.

1. Marcus, R. A. & Sutin, N. (1985) *Biochim. Biophys. Acta* **811,** 265–322.
2. Sigel, H. & Sigel, A., eds. (1991) *Metal Ions in Biological Systems* (Dekker, New York), Vol. 27.
3. Meyer, T. J. & Newton, M. D. (1993) *Chem. Phys.* **176,** 289–649 (special issue on electron transfer).
4. Bendall, D. S., ed. (1996) *Protein Electron Transfer* (BIOS Publishers, Oxford).
5. Kuznetsov, A. M. & Ulstrup, J. (1999) *Electron Transfer in Chemistry and Biology: An Introduction to the Theory* (Wiley, Chichester, U.K.), in press.
6. Moser, C. C., Page, C. C., Chen, X. B. & Dutton, P. L. (1997) *J. Biol. Inorg. Chem.* **2,** 393–398.
7. Winkler, J. R. & Gray, H. B. (1997) *J. Biol. Inorg. Chem.* **2,** 399–404 and references therein.

8. Finklea, H. A. (1996) *in Electroanalytical Chemistry*, Bard, A. J. & Lund, H., eds. (Dekker, New York), Vol. 19, pp. 109–335.
9. Smalley, J. F., Feldberg, S. W., Chidsey, C. E. D., Lindford, M. R., Newton, M. R. & Liu, Y.-P. (1995) *J. Phys. Chem.* **99,** 13141–13149.
10. Beratan, D. N., Betts, J. N. & Onuchic, J. N. (1991) *Science* **252,** 1285–1288.
11. Kuznetsov, A. M., Ulstrup, J. & Vigdorovich, M. V. (1993) *Chem. Phys.* **176,** 539–554.
12. Medvedev, E. S. & Stuckebruchov, A. A. (1997) *J. Chem. Phys.* **107,** 3821–3831.
13. Kharkats, Y. I., Kuznetsov, A. M. & Ulstrup, J. (1995) *J. Phys. Chem.* **99,** 13545–13554.
14. Chen, C. J. (1991) *Introduction to Scanning Tunneling Microscopy* (Oxford Univ. Press, Oxford).
15. Magonov, S. N. & Wangbo, M.-H. (1996) *Surface Analysis with STM and AFM* (Verlag Chemie, Weinheim, Germany).
16. Louder, D. R. & Parkinson, B. A. (1994) *Anal. Chem.* **66,** 84R–105R.
17. Sautet, P. (1997) *Chem. Rev.* **97,** 1097–1116.
18. Joachim, C. (1991) *New J. Chem.* **15,** 223–229.
19. Joachim, C. & Vinuesa, J. F. (1996) *Europhys. Lett.* **39,** 635–640 and references therein.
20. Samanta, M. P., Tian, W., Henderson, J. I., Datta, S. & Kubiak, C. P. (1996) *Phys. Rev. B* **53,** R7626–R7629.
21. Datta, S., Tian, W., Hong, S., Reifenberger, R., Henserson, J. I. & Kubiak, C. P. (1997) *Phys. Rev. Lett.* **79,** 2530–2533.
22. Ohtani, H., Wilson, R. J., Chiang, S. & Mate, C. M. (1988) *Phys. Rev. Lett.* **60,** 2398–2401.
23. Weiss, P. S. & Eigler, D. N. (1993) *Phys. Rev. Lett.* **71,** 3139–3142.
24. Hallmark, V. M., Chang, S., Meinhardt, K.-P. & Hafner, K. (1993) *Phys. Rev. Lett.* **70,** 3740–3743.
25. Joachim, C., Gimzewski, J. K., Schlitter, R. R. & Chauney, C. (1995) *Phys. Rev. Lett.* **74,** 2102–2105.
26. Poirier, G. E. (1997) *Chem. Rev.* **97,** 1117–1127.
27. Bumm, L. A., Arnold, J. J., Cygan, M. T., Dunbar, T. D., Burgin, T. P., Jones, L., II, Allara, D. L., Tour, J. M. & Weiss, P. S. (1996) *Science* **271,** 1705–1707.
28. Dhirani, A., Lin, P.-H., Guyot-Sionnest, P., Zehner, R. W. & Sita, L. R. (1997) *J. Chem. Phys.* **106,** 5249–5253.
29. Lu, X. & Hipps, K. W. (1997) *J. Phys. Chem.* **101,** 5391–5396.
30. Arscott, P. G. & Bloomfield, V. A. (1993) in *STM and SFM in Biology*, Marti, O. & Amrein, M., eds. (Academic, San Diego), pp. 259–272.
31. Andersen, J. E. T., Møller, P., Pedersen, M. V. & Ulstrup, J. (1995) *Surf. Sci.* **325,** 193–205.
32. Gewirth, A. & Siegenthaler, H., eds. (1995) *Nanoscale Probes of the Solid/Liquid Interface* (Kluwer, Dordrecht, The Netherlands).
33. Gewirth, A. & Niece, B. K. (1997) *Chem. Rev.* **97,** 1129–1162.
34. Danilov, A. I. (1995) *Russ. Chem. Rev.* **64,** 767–781.
35. Ota, I., Inukai, J. & Ito, M. (1993) *Chem. Phys. Lett.* **203,** 99–103.
36. Pan, J., Tao, N. J. & Lindsay, S. M. (1993) *Langmuir* **9,** 1556–1560.
37. Hobara, D., Ota, M., Imabayashi, S., Niki, K. & Kakiuchi, T. (1998) *J. Electroanal. Chem.* **444,** 113–119 and references therein.
38. Lindsay, S. M., Tao, N. J., DeRose, J. A., Oden, P. I., Lyubchenko, Y. L., Harrington, R. E. & Shlyakhtenko, L. (1992) *Biophys. J.* **61,** 1570–1584.
39. Lindsay, S. M. & Tao, N. J. (1993) in *STM and SFM in Biology*, Marti, O. & Amrein, M., eds. (Academic, San Diego), pp. 229–257.
40. Wandlowski, T., Lampner, D. & Lindsay, S. M. (1996) *J. Electroanal. Chem.* **404,** 215–226.
41. Höltze, M. H., Wandlowski, T. & Kolb, D. M. (1995) *Surf. Sci.* **335,** 281–290.
42. Höltze, M. H., Wandlowski, T. & Kolb, D. M. (1995) *J. Electroanal. Chem.* **394,** 271–275.
43. Kunitake, M., Batina, N. & Itaya, K. (1995) *Langmuir* **11,** 2377–2380.
44. Tao, N. J., Gardenas, G., Cunha, F. & Shi, Z. (1995) *Langmuir* **11,** 4445–4448.
45. Bunge, E., Nichols, R. J., Roelfs, R., Meyer, H. & Baumgärtel, H. (1996) *Langmuir* **12,** 3060–3066.
46. Tao, N. J. & Shi, Z. (1994) *Surf. Sci.* **321,** L149–L153.
47. Tao, N. (1996) *Phys. Rev. Lett.* **76,** 4066–4069.
48. Han, W., Durantini, E. N., Moore, T. A., Moore, A. L., Gust, D., Rez, P., Leatherman, G., Deely, G. R., Tao, N. & Lindsay, S. M. (1997) *J. Phys. Chem.* **101,** 10719–10725.
49. Friis, E. P., Kharkats, Y. I., Kuznetsov, A. M. & Ulstrup, J. (1998) *J. Phys. Chem.* **102,** 7851–7859.
50. Radmacher, M., Fritz, M., Hansma, H. G. & Hansma, P. K. (1994) *Science* **265,** 1577–1579.
51. Rief, M., Gautel, M., Osterhelt, F., Fernandezz, J. M. & Gaub, H. E. (1997) *Science* **276,** 1109–1112.
52. Li, H., Rief, M., Osterhelt, F. & Gaub, H. E. (1998) *Adv. Mat.* **3,** 316–318.
53. Friis, E. P., Andersen, J. E. T., Madsen, L., Bonander, N., Møller, P. & Ulstrup, J. (1997) *Electrochim. Acta* **42,** 2889–2897, and erratum (1998) **43,** 2889–2897.
54. Zhang, J., Chi, Q., Dong, S. & Wang, E. (1996) *Bioelectrochem. Bioeng.* **39,** 267–274.
55. Andersen, J. E. T., Olesen, K. G., Danilov, A. I., Foverskov, C. E., Møller, P. & Ulstrup, J. (1997) *Bioelectrochem. Bioeng.* **44,** 57–63.
56. Friis, E. P., Andersen, J. E. T., Madsen, L. L., Møller, P. & Ulstrup, J. (1997) *J. Electroanal. Chem.* **431,** 35–38.
57. Farver, O., Wherland, S. & Pecht, I. (1994) *J. Mol. Biol.* **269,** 22933–22936.
58. Guo, L.-H. & Hill, H. A. O. (1991) *Adv. Inorg. Chem.* **36,** 341–375.
59. Farver, O. (1996) in *Protein Electron Transfer*, Bendall, D., ed. (BIOS Publishers), p. 161.
60. Vijgenboom, E. & Canters, G. W. (1997) *Microbiology* **143,** 2853–2861.
61. Nar, H., Messerschmidt, A. & Huber, R. (1991) *J. Mol. Biol.* **221,** 765–772.
62. Kraulis, P. (1991) *J. Appl. Cryst.* **24,** 946–950.
63. Chergui, M., ed. (1995) *Femtochemistry: Ultrafast Chemical and Physical Processes in Molecular Systems* (World Scientific, Singapore).
64. Manz, J. & Wöste, L., eds. (1995) *Femtosecond Chemistry* (Verlag Chemie, Weinheim, Germany), Vols. 1–2.
65. Dogonadze, R. R. & Kuznetsov, A. M. (1975) *Prog. Surf. Sci.* **6,** 1–42.